Geochemistry, Geophysics, Geosystems®

RESEARCH ARTICLE
10.1029/2023GC011007

Systematic Across-Arc Variations of Molybdenum Isotopes in a Fluid-Dominated Subduction Zone System

M. Willbold[1] **and N. Messling**[1]

[1]Abteilung Geochemie und Isotopengeologie, Fakultät für Geowissenschaften und Geographie, Universität Göttingen, Göttingen, Germany

Abstract Mass-dependent Mo isotope variations are a promising new tracer to study magmatic processes in different geological settings. We report the first Mo isotope data for the Kamchatka arc system in the Northwest Pacific, comprising basaltic lavas of a complete Southeast-Northwest traverse from the volcanic arc front through to the back arc region. The majority of volcanic centers investigated directly override the Hawaii-Emperor Seamount Chain, which is currently being subducted underneath the arc system. Our Mo isotope data show systematic trends with Ce/Pb, Ce/Mo, Nb/Zr, La/Sm, and $^{143}Nd/^{144}Nd$ ratios from the volcanic arc front to the back arc. Arc front lavas have higher $\delta^{98/95}Mo$ and lower Ce/Pb, Ce/Mo, Nb/Zr, La/Sm compared to back arc lavas. Because the involvement of subducted sediments can be excluded, we attribute the observed variations to a change in the mantle source composition from the arc front to the back arc regions. The isotopic and chemical budget of arc front lavas is dominated by a slab fluid component (high $\delta^{98/95}Mo$, low Ce/Pb, Ce/Mo), whereas mantle-like Ce/Pb, Ce/Mo, elevated Nb/Zr and La/Sm in the back arc samples suggest an enriched mantle source. Combined $\delta^{98/95}Mo$, Nd, and Pb isotope data in back arc lavas are very similar to those observed for modern ocean island basalts from Hawaii. We thus explore the possibility that the back arc mantle was contaminated by a Hawaii-type, enriched asthenospheric mantle component from the subducted Hawaii-Emperor Seamount Chain.

Plain Language Summary In subduction zones, tectonic plates—tens of kilometers thick and making up the outer shell of our planet—are on a collision course. Although the absolute convergence rates of these plates are minute (a few cm/year), the forces in this process are so large that one plate is pushed under the other, causing the lower plate to be recycled into the Earth's mantle over time scales of millions of years. The tangible consequences are high-magnitude earthquakes and large-volume volcanic eruptions along these convergent plate margins. It is thus important to better understand the geological processes that operate in subduction zones. Here, we have studied the chemical and isotopic composition of volcanic rocks from the Kamchatka subduction zone. Our results confirm that water, locked into the subducting plate while residing on the surface, is released into the hot, overlying mantle after subduction, causing the formation of large volumes of magma that eventually erupt in volcanoes on the Kamchatka Peninsula. Our data also indicate that the subducting plate, once pushed into the mantle, is being ripped apart, allowing buoyant mantle material from greater depth to rise and contribute to the large-scale volcanism observed along this convergent plate margin.

Key Points:

- Molybdenum isotope systematics in arc basalts from Kamchatka are consistent with presence of a slab-derived fluid in their mantle source
- Back arc basalts also show contribution from a geochemically enriched source
- Combined Mo, Nd, and Pb isotope and trace element data for back arc basalts suggest involvement of Hawaii-type asthenospheric mantle

Supporting Information:

Supporting Information may be found in the online version of this article.

Correspondence to:

M. Willbold,
matthias.willbold@uni-goettingen.de

Citation:

Willbold, M., & Messling, N. (2023). Systematic across-arc variations of molybdenum isotopes in a fluid-dominated subduction zone system. *Geochemistry, Geophysics, Geosystems*, *24*, e2023GC011007. https://doi.org/10.1029/2023GC011007

Received 20 APR 2023
Accepted 10 AUG 2023

Author Contributions:

Conceptualization: M. Willbold
Data curation: M. Willbold
Funding acquisition: M. Willbold
Investigation: M. Willbold, N. Messling
Methodology: M. Willbold
Project Administration: M. Willbold
Writing – original draft: M. Willbold
Writing – review & editing: N. Messling

1. Introduction

Over the past few years, the use of mass-dependent Mo isotope variations in studying magmatic processes has gained considerable traction. This is because under ambient mantle conditions, Mo predominantly exists in its Mo^{6+} valence state (O'Neill & Eggins, 2002) and is therefore a lithophile, highly incompatible element that is geochemically fractionated between the Earth's mantle and crust (Greaney et al., 2018; Greber et al., 2015; Newsom & Palme, 1984; Palme & O'Neill, 2014; Rudnick & Gao, 2014). From a global perspective, the depleted mantle has a moderate but resolvable sub-chondritic $\delta^{98/95}Mo$ of −0.22‰ (Bezard et al., 2016; Hin et al., 2022; McCoy-West et al., 2019), with chondrites having an average $\delta^{98/95}Mo = -0.15‰$ (Burkhardt et al., 2014; Liang et al., 2017). In contrast, the Earth's upper continental crust appears to have a super-chondritic bulk Mo isotope composition of ca. +0.15‰ (Willbold & Elliott, 2017). Here, $\delta^{98/95}Mo$ denotes the parts-per-thousand deviation in $^{98}Mo/^{95}Mo$ determined for a particular sample relative to that of the National Institute of Standards and Technology (NIST) standard reference material 3134. The observed dichotomy between the mantle and the continental crust is intriguing because mass-dependent Mo isotope fractionation should be near-absent in magmatic

systems owing to the small relative mass difference between Mo isotopes and the high temperatures, under which magmatic processes operate (Bigeleisen & Mayer, 1947; Gaschnig et al., 2021a; Urey, 1947; Yang et al., 2015).

In this context, measured Mo abundances and isotope compositions in slab fluid-dominated mafic arc lavas positively covary with tracers of fluid addition (Freymuth et al., 2015; Gaschnig et al., 2017; König et al., 2016; Villalobos-Orchard et al., 2020). This is in line with experimentally constrained mobility of Mo metamorphic fluids at slab conditions (Bali et al., 2012; Green & Adam, 2003; König et al., 2016) and also suggests that the high-$\delta^{98/95}$Mo signature observed in fluid-rich arc basalts are derived from redox-driven reaction of the fluid with the subducted crust under metamorphic conditions (Ahmad et al., 2021; Chen et al., 2019; Freymuth et al., 2015; Gaschnig et al., 2017; König et al., 2016; Villalobos-Orchard et al., 2020; Willbold & Elliott, 2017). Overall, there is an increasing data set for Mo isotope data in arc rocks. However, lavas from back arc systems are yet to be appropriately characterized (X. Li et al., 2021a). In this context, the Kamchatka arc system provides a unique setting, as it is one of the largest across-arc systems worldwide with contemporary magmatic activity from the volcanic arc front into the back arc region. It therefore offers an ideal opportunity to constrain the continuous change in the Mo isotope inventory of arc-related magmas from a fluid-dominated volcanic front to the mantle-dominated back arc region in a single arc system and with a limited number of potential geochemical sources and near-constant subduction parameters. In this contribution we will thus explore the different geological processes that determine the Mo isotope compositions of arc lavas observed across an entire system. To this end, our results contribute to a better understanding of the Mo isotope systematics in modern subduction zones and a reliable interpretation of the Mo isotope data in complex present-day subduction zones or arc systems that are preserved in the geological record (e.g., Ahmad et al., 2021, 2022; Casalini et al., 2019; Fang et al., 2022; H. Y. Li et al., 2019; H. Q. Liu et al., 2022; Ma et al., 2022; Rojas-Kolomiets et al., 2023; Yu et al., 2022; Zhang et al., 2019, 2020).

2. Geological Setting and Sample Selection

The Kamchatka arc forms part of the Circum-Pacific Volcanic Belt (Figure 1). Its volcanic activity is caused by the subduction of the ca. 90–105 Ma old oceanic Pacific plate under the Eurasian plate at a rate of currently ca. 9 cm/year (Geist & Scholl, 1994). To the South, the arc continues into the Kuril volcanic arc, whereas to the North it is terminated by the Aleutian-Kamchatka triple junction through a series of transform faults (Gorelchik et al., 1997; Yogodzinski et al., 1995, 2001). Here, the plate motion changes from convergent to strike-slip between the Pacific and the North American plate. Early magmatic rocks in the Kamchatka arc system date back to the Cretaceous. Volcanic activity increased during the Pliocene to Lower Pleistocene with the emplacement of plateau basalts and culminated in the Upper Pleistocene to Holocene (Churikova et al., 2001). The present dip angle of the subducted plate shallows from 55° in the South to 35° in the North, probably related to the subduction of the Hawaii-Emperor Seamount Chain below the Northern part of Kamchatka. This change in dip angle, as well as the broadening of crustal extension of the Central Kamchatka Depression (CKD) north of ca. 55°N, causes a shift of the volcanic activity in the arc from the East to the West (Figure 1). Today, this area is one of the volcanically most active regions on Earth with more than 34 active volcanoes and abundant eruptions of mafic arc lavas (Kepezhinkas et al., 1997).

Active arc volcanism in Kamchatka can be divided into three zones that run sub-parallel to the trench (Figure 1): Volcanic centers of the Eastern Volcanic Front (EVF) comprise the frontal arc of the Kamchatka system. Further to the West lies the CKD, which includes the large active cluster of the Klyuchevskoy Group and the Shiveluch Group in the Northern Central Kamchatka Depression (NCKD). This region is one of the most productive parts of the subduction zone and comprises ca. 50% of melt volume of the active volcanoes of the entire Kuril-Kamchatka arc (Ishikawa et al., 2001). The Sredinny Ridge (SR) represents the back arc of the Kamchatka system, some 400 km behind the present trench with Holocene volcanism at the Ichinsky volcano (Volynets et al., 2009). Along the arc, crustal thickness increases from 20 km in the South to 42 km in the North (Balesta, 1991; Gorbatov, 1997). Above the subducted Hawaii-Emperor Seamount Chain and across the arc, crustal thickness varies from ca. 30 km under the SR to ca. 42 km underneath the CKD and the Klyuchevskaya Group, where the crust-mantle transition is marked by a ca. 10 km thick zone most likely related to massive underplating of basaltic melts (Balesta, 1991). This would explain the surprising thick crust of the CKD, given that this zone is considered a rift-like structure, for which an otherwise thinned crust would be expected (Churikova et al., 2001). Such a model is supported by seismic evidence that suggests the existence of active magma reservoirs within the Kamchatka crust

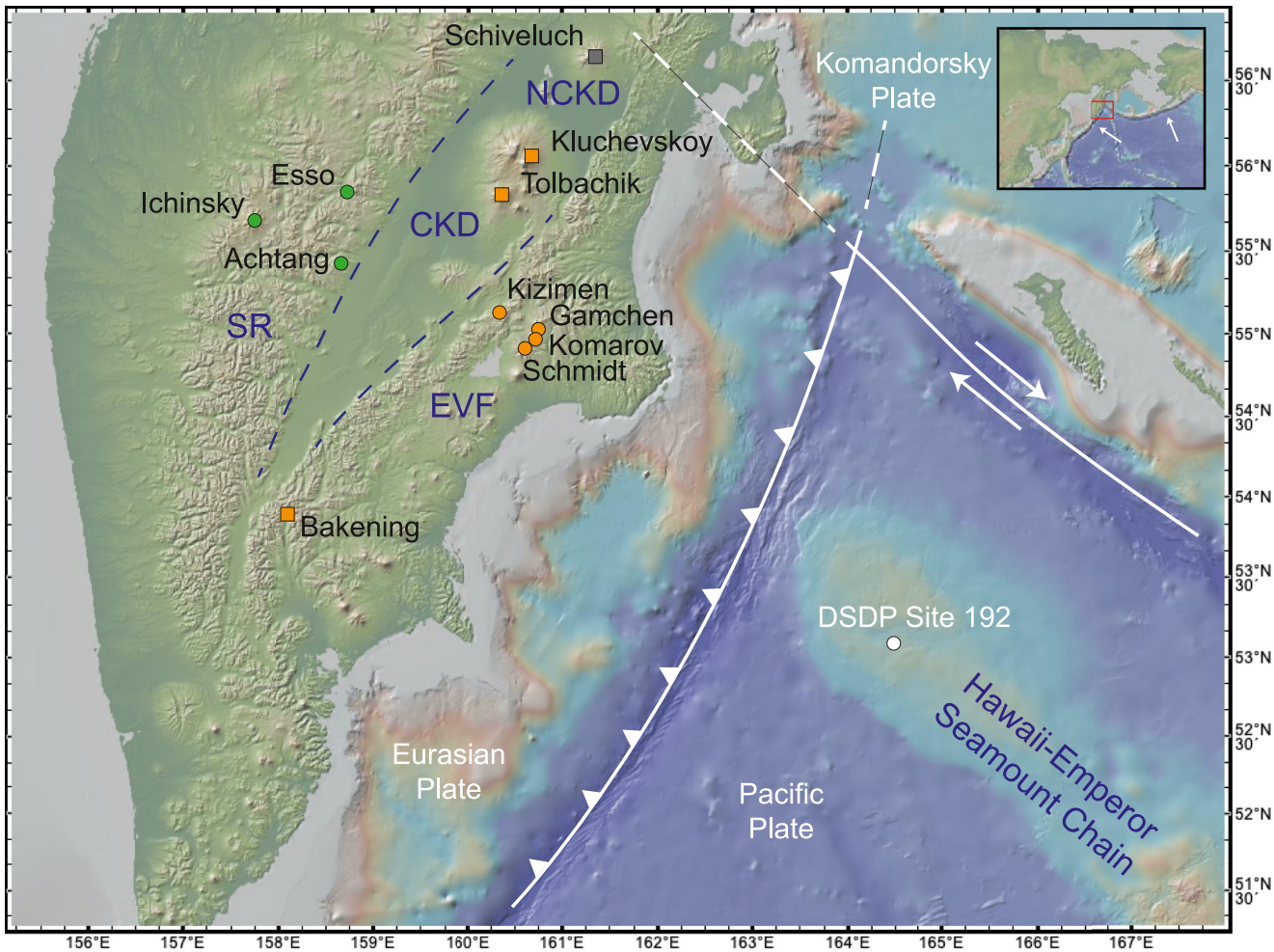

Figure 1. Map of the southern Kamchatka peninsula showing the locations of investigated volcanoes. Most samples come from a Southeast-Northwest transect overriding the Hawaii-Emperor Seamount Chain that is currently being subducted underneath the Eurasian Plate. EVF: Eastern Volcanic Front, CKD: Central Kamchatka Depression, SR: Sredinny Ridge (back arc), NCKD: Northern Central Kamchatka Depression. After Churikova et al. (2001). The location of DSDP Site 192 drill core is also shown (see text). Base map from https://www.geomapapp.org.

with depths ranging from ca. 2 km below the Avachinsky and Tolbachik volcanoes through to the transition zone depths of ca. 20 km underneath the Bezymianny volcano (Balesta, 1991). At mantle depths, the seismic zone of the subducted plate is situated about 100–140 km beneath the EVF, 100–200 km below the CKD and extents to a depth of 400 km in the SR (Gorbatov, 1997).

All Kamchatka magmas display rather uniform Pb isotope ($^{206}Pb/^{204}Pb$ = 18.15–18.30, $^{207}Pb/^{204}Pb$ = 15.4 5–15.48, $^{208}Pb/^{204}Pb$ = 37.74–37.95) as well as Sr isotope compositions ($^{87}Sr/^{86}Sr$ = 0.70334–0.70366) (Churikova et al., 2001; Dorendorf, Wiechert, & Wörner, 2000). Together with comparatively low ^{10}Be abundances ($<1.2 \times 10^6$ at/g), this suggests that the trace element budget of Kamchatka lavas is mainly controlled by fluids derived from the subducted plate and less so by subducted sediments (Churikova, Wörner, Mironov, & Kronz, 2007; Churikova et al., 2001; Dorendorf, Wiechert, & Wörner, 2000; Kersting & Arculus, 1995; Münker et al., 2004). The samples of this study come from a 210 km Southeast to Northwest transect across the Kamchatka arc (Churikova et al., 2001) encompassing its three structural units, the EVF, the CKD and the SR, mostly following the trail of the subducted Hawaii-Emperor Seamount Chain (Figure 1). Most of the samples were previously characterized according to their geochemistry as well as their Sr, Nd and Pb isotopic composition (Churikova, Wörner, Mironov, & Kronz, 2007; Churikova et al., 2001; Dorendorf, Wiechert, & Wörner, 2000; Münker et al., 2004). Based on these data, care has been taken to limit the sample selection of this study to mafic lithologies in order to minimize any potential effect of fractional crystallization or assimilation processes on Mo

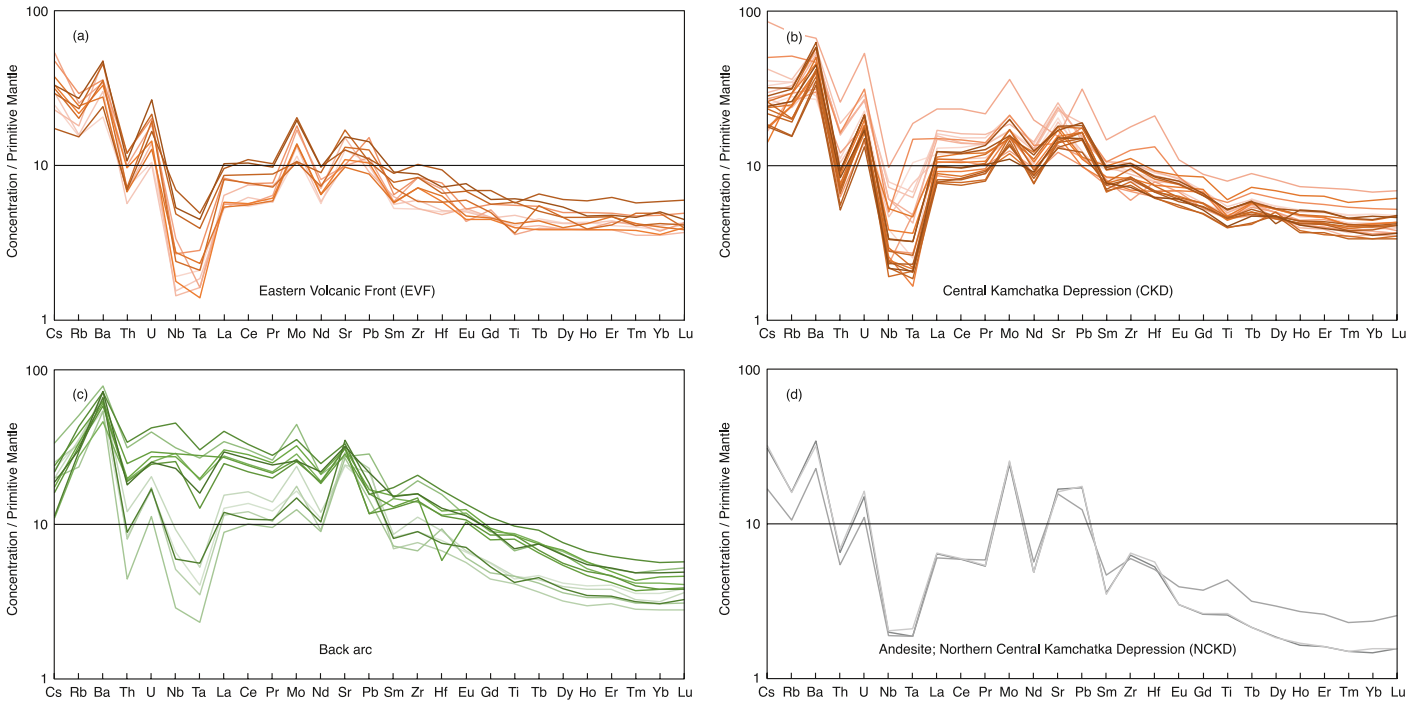

Figure 2. Primitive upper mantle (PUM)-normalized trace element patterns of Kamchatka lavas of this study. (a) Eastern Volcanic Front (EVF), (b) Central Kamchatka Depression (CKD), (c) Back arc (Sredinny Ridge—SR) and (d) andesites from the Northern Central Kamchatka Depression (NCKD). Data from Churikova et al. (2001) and this study. Values for PUM were taken from Palme and O'Neill (2014).

isotope distributions (Freymuth et al., 2015; Villalobos-Orchard et al., 2020). The samples comprise basalts from the volcanoes of Gamchen, Schmidt, Komarov and Kizimen (EVF), the Klyuchevskoy, Tolbachik (CKD) and Schiveluch volcanoes (NCKD), as well as from the Esso and Achtang region and the Ichinsky back arc volcanoes (SR). For the purpose of this study, we have allocated the Bakening volcanic center with its transitional CKD-EVF character (Churikova et al., 2001) to the CKD group. For comparison (see below), the data set also includes data for three andesites from Schiveluch volcano in the NCKD. The maximum arc width is found where the Hawaii-Emperor Seamount Chain is being subducted underneath the Kamchatka arc (Figure 1). Accordingly, the across-arc distance of active volcanism covered by our Mo isotope sample set is one of the widest found in any arc setting today.

3. Results

High-precision Mo isotope data for all samples have been acquired at the Department of Geochemistry and Isotope Geology, University of Göttingen. Existing trace element and $^{143}Nd/^{144}Nd$ data (Churikova et al., 2001; Norman & Garcia, 1999) have been supplemented by newly acquired data for critical samples where necessary. A detailed description of all analytical procedures is given in Supporting Information S1. All data, together with relevant measures of quality control, are reported in Table S1. According to their SiO_2 and alkaline element composition (Le Maitre et al., 1989), all EVF and CKD samples are classified as basalts and basaltic andesites, whereas back arc samples also include trachybasalts and basaltic trachyandesites.

All EVF and CKD samples show rather uniform Primitive Upper Mantle (PUM)-normalized trace element patterns (Figure 2) typical for a subduction zone setting (Pearce & Peate, 1995). These include a general enrichment of large-ion-lithophile element (LILE) concentrations over light rare-earth element (LREE) concentrations, the enrichment of LREE over heavy REE (HREE) concentrations and depletion of high-field strength elements (HFSE) Nb and Ta relative to La and Th. In detail, however, small but systematic variations between the EVF and CKD exist (also see Churikova et al., 2001). Samples from the EVF show less pronounced and more variable Nb depletion compared to samples from the CKD. The average PUM-normalized $(Nb/La)_{PUM}$ in EVF samples is 0.43 ± 0.16 (1SD; n = 11) compared to the average $(Nb/La)_{PUM}$ 0.33 ± 0.08 in CKD samples (n = 24). Note

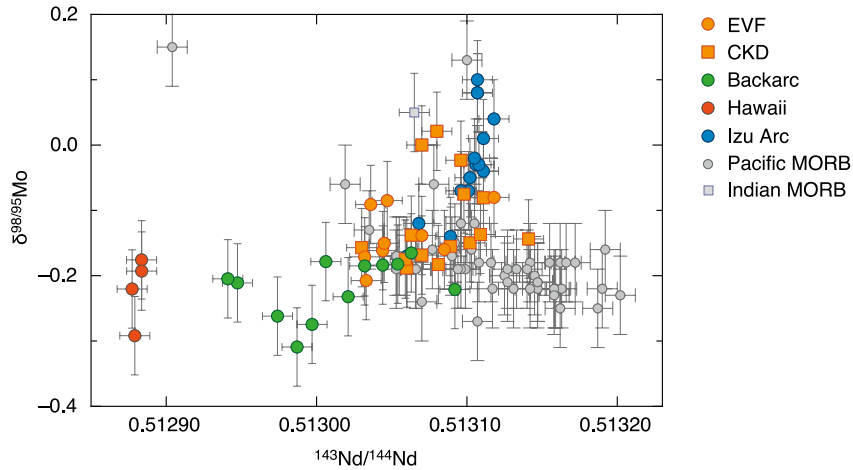

Figure 3. Plot of $^{143}Nd/^{144}Nd$ against $\delta^{98/95}Mo$ (in ‰) for samples from Kamchatka (Table S1), as well as from the Izu arc (Villalobos-Orchard et al., 2020), Pacific and Indian MORB (Bezard et al., 2016; Chen et al., 2022; Hin et al., 2022; Liang et al., 2017) and Hawaii (Table S1). Uncertainties indicate 2SD confidence intervals of repeated measurements of geological reference materials (see Supporting Information S1).

that, PUM-normalized trace element ratios of 1 express relative parity between the two elements (see Figure 2), whereas lower and higher values express depletion and enrichment, respectively.

Compared to EVF and CKD samples, samples from the back arc (i.e., the SR group; $n = 12$) show less pronounced relative LILE enrichments and HFSE depletion in their trace element patterns, with an average $(Rb/La)_{PUM}$ of 1.8 ± 0.7 and $(Nb/La)_{PUM}$ of 0.68 ± 0.34 compared to 2.7 ± 0.7 and 0.36 ± 0.12, respectively, in EVF and CKD samples. However, back arc samples are generally more enriched in incompatible element over less incompatible element abundances as expressed by their elevated chondrite-normalized $(La/Yb)_{CI}$ of 5.5 ± 1.5, compared to the EVF and CKD samples (average $(La/Yb)_{CI} = 2.4 \pm 0.8$). Also, $(Nb/Zr)_{PUM}$ ratios in back arc samples tend to be higher (average 1.2 ± 0.7) than in the EVF and CKD samples (average 0.43 ± 0.15; also see Figure 2).

Andesites from the Schiveluch volcano in the NCKD ($n = 3$; Table S1) show relative enrichment in LILE and LREE as well as relative depletion in HFSE, typical of andesitic rocks from subduction zone settings, but are additionally marked by elevated Sr/Y ratios (average 45) at low Y concentrations (average 8.3 µg/g). High Sr/Y and MREE/HREE ratios reflect a so-called "adakitic" trace element signature that has been related to partial melting of subducted oceanic crust (Yogodzinski et al., 2001). A comprehensive description of the petrography and geochemistry of the samples analyzed here is given in Churikova et al. (2001), Dorendorf, Churikova, et al. (2000), Dorendorf, Wiechert, and Wörner (2000), and Yogodzinski et al. (2001).

There is considerable overlap in radiogenic $^{143}Nd/^{144}Nd$ ratios between EVF and CKD samples (Figure 3), yet they have on average higher $^{143}Nd/^{144}Nd$ (average 0.513074 ± 0.000061, 2SD) compared to samples from the back arc (average 0.513013 ± 0.000093, 2SD; also see Figure 3). Molybdenum isotope ratios in samples from Kamchatka vary between $\delta^{98/95}Mo = -0.31$ and $+0.02$‰ and show a distribution similar to that observed for $^{143}Nd/^{144}Nd$ ratios (Figure 3) with EVF and CKD samples having an average higher $\delta^{98/95}Mo$ (average -0.13 ± 0.13‰; 2SD) compared to the average value for the back arc samples ($\delta^{98/95}Mo = -0.22 \pm 0.09$‰; 2SD). This results in a trend between Nd and Mo isotope data for the Kamchatka sample set.

4. Discussion

4.1. Effect of Fractional Crystallization and Crustal Assimilation on the Mo Isotope Variation of Kamchatka Basalts

It has been proposed that continuous intra-arc fractionation of isotopically light amphibole during magmatic differentiation of mafic parental magmas decreases Dy/Yb whilst increasing La/Yb ratios and $\delta^{98/95}Mo$ values in the residual, high-SiO_2 melts (Davidson et al., 2013; Voegelin et al., 2014; Wille et al., 2018). Our focus on mafic samples helps to minimize such effects but we cannot a priori assume that the observed $\delta^{98/95}Mo$ variations in

our data set are insensitive to differences in the degree of fractional crystallization between individual samples. Figures S1a and S1b in Supporting Information S1 shows $\delta^{98/95}$Mo data plotted against MgO content as a measure of the degree of fractional crystallization. Data for the three different sample groups (EVF, CKD, back arc) define a cluster between 4 and 10 wt.% MgO and no significant trend with $\delta^{98/95}$Mo. Weak negative trends between $\delta^{98/95}$Mo and SiO_2 and Dy/Yb are visible (Figures S1b and S1c in Supporting Information S1). However, similar trends in the same direction are observed when plotting SiO_2 and Dy/Yb ratios against $^{143}Nd/^{144}Nd$ (Figures S1e and S1f in Supporting Information S1), hinting at a possible source effect that controls Dy/Yb and SiO_2 (and also $\delta^{98/95}$Mo; see below) in the samples rather than fractionation of amphibole. In addition, the trend of $\delta^{98/95}$Mo data with $^{143}Nd/^{144}Nd$ values (Figure 3) is unlikely to be controlled by fractional crystallization processes and also rules out partial melting effects (cf. McCoy-West et al., 2019) as a driver of Mo isotope variability in the mantle-sourced Kamchatka basalts.

Churikova et al. (2001) used near-constant K_2O/Na_2O ratios at variable MgO contents on a much larger sample set (>90 lavas), which included samples of this study but also more differentiated rocks (andesites, dacites, and rhyolites), as an indicator for limited crustal assimilation in the Kamchatka magmas. Exceptions were some samples from the Tolbachik volcano (CKD). However, we do not observe any trend between $\delta^{98/95}$Mo and K_2O/Na_2O for our samples from this volcano (Figure S2 in Supporting Information S1). We therefore assume that these samples are also not affected by crustal assimilation. However, excluding these samples from the discussions below would not change the conclusions of this study. Overall, the combined considerations above suggest that the $\delta^{98/95}$Mo in the Kamchatka arc basalts are not controlled by shallow magmatic processes but reflect the Mo isotope composition of their respective sources in the mantle, in line with findings from other Mo isotope studies on mafic lavas (Freymuth et al., 2015, 2016; Gaschnig et al., 2017, 2021a; König et al., 2016; Rojas-Kolomiets et al., 2023; Villalobos-Orchard et al., 2020; Yang et al., 2015).

4.2. Slab Contribution to the Mo Budget of the Eastern Volcanic Front (EVF) and Central Kamchatka Depression (CKD) Magmas

Enrichment of LILE over LREE, high LREE/HREE ratios, together with concomitant $(Nb/La)_{PUM} < 1$ and $(Nb/Zr)_{PUM} < 1$ in arc basalts are generally assumed to reflect the incorporation of slab-derived material in their sources (Elliott et al., 1997, 2007; Gill, 1981; Hawkesworth et al., 1991; Spandler & Pirard, 2013). For the Kamchatka arc system, the uniform and unradiogenic $^{206}Pb/^{204}Pb$ composition of the lavas, the lack of correlation between Pb and Nd isotopes with indicators of subducted sediments (e.g., Th/La and Sr isotopes) as well as high Ba/Th at low Th contents (<3 μg/g) have previously been used to argue for a dominant aqueous slab fluid component and the absence of a significant contribution from subducted sedimentary components in the source of the arc basalts (Churikova, Wörner, et al., 2007; Churikova et al., 2001; Kersting & Arculus, 1995; H. Liu et al., 2020; Münker et al., 2004; Shu et al., 2022). Within each group—(a) EVF and CKD arc basalts on one hand and (b) back arc basalts on the other—our measured $\delta^{98/95}$Mo values also do not correlate with typical markers for sediment input, such as Pb isotopes or chondrite-normalized $(La/Sm)_{CI}$ (Figures S3 and S1d in Supporting Information S1). Values of $\delta^{98/95}$Mo for EVF and CKD samples vary independently from both, $^{206}Pb/^{204}Pb$ and $(La/Sm)_{CI}$ ratios, ranging between −0.25 and 0.02‰, while $\delta^{98/95}$Mo values for back arc samples are rather constant at −0.17 to −0.31‰ for a range of $(La/Sm)_{CI}$ (1.0–2.5). A similar observation is made for combined $\delta^{98/95}$Mo and $(Nb/Zr)_{PUM}$ data (Figure 4). Thus, while the observed relative increase in the enrichment of immobile incompatible elements in the basalts—from (a) the arc (EVF, CKD) toward (b) the back arc—seems to be geographically related, the variation of $\delta^{98/95}$Mo within each group is unlikely to be dominated by partial melts of a slab- or sediment component.

In contrast, basalts from Kamchatka show trends of $\delta^{98/95}$Mo with Ce/Pb, Ce/Mo, and Ba/Th (Figure 4). Notably, the Kamchatka data extend similar trends observed in mafic lavas from the Izu arc, where decreasing $\delta^{98/95}$Mo correlate with increasing Ce/Pb and Ce/Mo as well as decreasing Ba/Th (Villalobos-Orchard et al., 2020). Along this trend, EVF and CKD arc lavas are similar to Izu arc lavas. They have high $\delta^{98/95}$Mo and Ba/Th ratios as well as low Ce/Pb and Ce/Mo ratios. Back arc basalts have lower $\delta^{98/95}$Mo as well as higher Ce/Pb and Ce/Mo ratios. The element ratios Ce/Mo, Ce/Pb, Ba/Th are a diagnostic feature for the involvement of a slab fluid phase because these element pairs behave near-identically during mantle melting but Mo, Pb, and Ba are more mobile in slab fluids than Ce and Th (Bali et al., 2012; Elliott et al., 1997; Hofmann et al., 1986; Keppler, 1996; McCulloch & Gamble, 1991; Newsom & Palme, 1984; Newsom et al., 1986). The addition of such fluids to a mantle source will

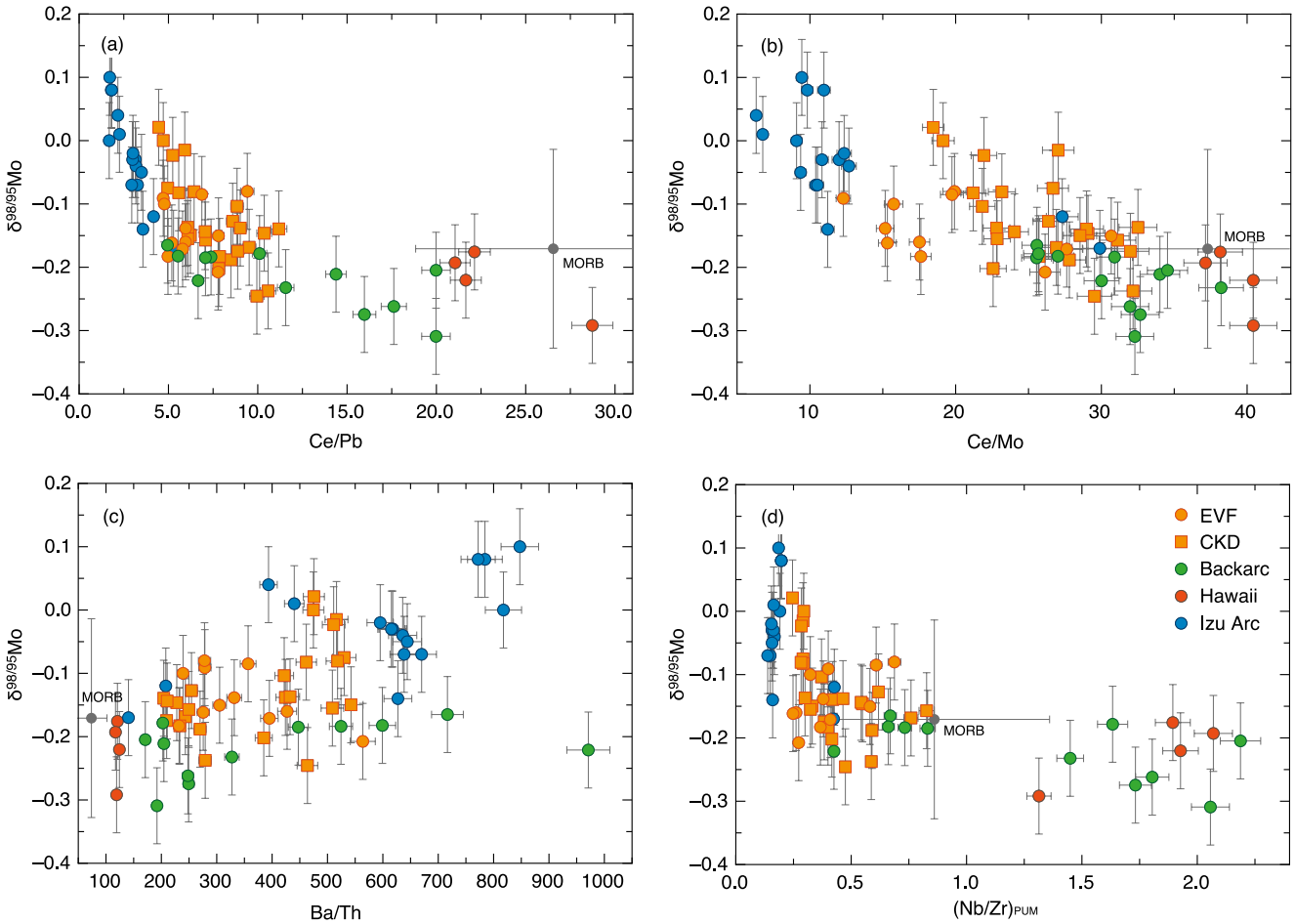

Figure 4. Plots of $\delta^{98/95}$Mo (‰) versus (a) Ce/Pb, (b) Ce/Mo, (c) Ba/Th, and (d) $(Nb/Zr)_{PUM}$ for samples from Kamchatka as well as from the Izu arc (Villalobos-Orchard et al., 2020) and Hawaii. Average compositions of Pacific and Indian MORB (Bezard et al., 2016; Chen et al., 2022; Hin et al., 2022; Liang et al., 2017) for reference.

thus cause its Ce/Mo and Ce/Pb to drop and Ba/Th to increase relative to the average mantle values (Hofmann et al., 1986; Newsom et al., 1986; Salters & Stracke, 2004; Workman & Hart, 2005). Therefore, the observed trends in the Kamchatka and Izu basalts provide a clear indication that $\delta^{98/95}$Mo in the EVF and CKD arc lavas are predominantly controlled by slab fluids. This is in good agreement with the findings of Freymuth et al. (2015) and Villalobos-Orchard et al. (2020), who suggested a fluid control on the Mo budget in similarly fluid-dominated arc basalts from the Mariana and Izu subduction zones. In this context, the marginally less well-defined trend between $\delta^{98/95}$Mo and Ba/Th (Figure 4) is most likely a reflection of the more variable Ba/Th in Mid-Ocean Ridge Basalts (MORB) (i.e., the source of Ba in the fluid), compared to more homogeneous Ce/Mo and Ce/Pb compositions. For instance, the single relative standard deviation of Ba/Th for Pacific and Indian MORB samples, for which combined $\delta^{98/95}$Mo and trace element data are available (Bezard et al., 2016; Chen et al., 2022; Hin et al., 2022; Liang et al., 2017), is 38%, compared to 29% for Ce/Mo and Ce/Pb. In addition, the mobilization of Mo in slab fluids critically depends on the presence of complexing agents (Bali et al., 2012), whereas Ba is a highly fluid-mobile element. As such, initial Ba/Th heterogeneity, a difference in fluid mobility between Ba and Mo, or a combination of both, could lead to a slight decoupling of the $\delta^{98/95}$Mo—Ba/Th systematic observed for our samples.

It has previously been demonstrated that Pb isotopes can be used to trace the source of slab-derived fluids (e.g., Avanzinelli et al., 2012; Miller et al., 1994; Shu et al., 2022). In this respect, the Pb isotope composition of Kamchatka arc lavas does not match the Pb isotope composition of drilled basalts and sediments from DSDP Site 192, sampling the altered crustal section of the Hawaii-Emperor Seamount Chain that is currently being subducted into the Kamchatka arc (Figure 5). The Pb isotope systematic of the Kamchatka arc lavas is

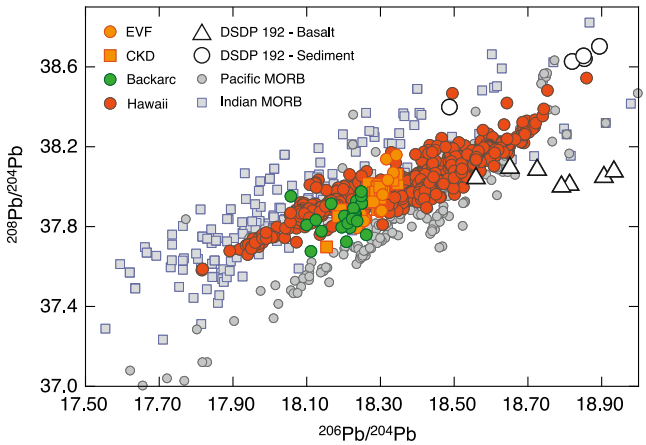

Figure 5. Plot of $^{208}Pb/^{204}Pb$ versus $^{206}Pb/^{204}Pb$ in arc and back arc volcanic rocks from the Southeast-Northwest transect in Kamchatka (Churikova et al., 2001; Dorendorf, Wiechert, & Wörner, 2000). The basaltic samples of this study are included in these data sets. Also shown are data for oceanic basalts and sediments from DSDP Site 192, sampling the upper altered section of the Hawaii-Emperor Seamount Chain crust currently being subducted under the transect (Regelous et al., 2003; Shu et al., 2022). Note that data for Kamchatka volcanic rocks firmly overlap with data for modern ocean island basalts from Hawaii (https://georoc.eu/georoc/new-start.asp; data retrieved October 2022) but not with data for the upper crustal section of subducted crust (basalts and sediments). Data for Pacific and Indian MORB from Stracke et al. (2005). See text for discussion.

therefore inconsistent with the derivation of a slab fluid component originating in altered, upper part of the subducted Hawaii-Emperor Seamount Chain crust. Unaltered sections of the Hawaii-Emperor Seamount Chain crust have not been recovered from DSDP Site 192. Yet, the latter may be accurately approximated by present-day ocean island basalts from Hawaii, as both, the current Hawaii archipelago as well as the Hawaii-Emperor Seamount Chain, were formed by the same mantle plume (Clague & Brent Dalrymple, 1994; Regelous et al., 2003; Tatsumoto, 1978). The Pb isotope data for Kamchatka arc lavas firmly overlap with those of modern ocean island basalts from Hawaii (Figure 5) and therefore suggest that the Pb budget of the Kamchatka arc lavas is predominantly sourced from the lower, less altered lithosphere of the subducted Hawaii-Emperor Seamount Chain (Figure 6a).

Not only is this conclusion in line with similar findings for the fluid source in the Mariana arc system (Avanzinelli et al., 2012; Freymuth et al., 2015), it also confirms the more general observation that large quantities of slab fluids are sourced from the deeper, serpentinized mantle lithosphere of the slab (Skora & Blundy, 2010; Spandler & Pirard, 2013; Till et al., 2011; van Keken et al., 2011). These serpentinites likely form as a result of the bending of the down-going plate during incipient subduction and the concomitant formation of deep-rooted fractures that penetrate into the lithospheric mantle (Ranero et al., 2003). Continued subduction to mantle depth then causes the lithospheric serpentinite layer to de-stabilize and to eventually release fluids upward into the overlying mafic crustal section (Walowski et al., 2015). Within this context, Chen et al. (2019) have shown that the high $\delta^{98/95}Mo$ values of the slab fluid are controlled by the stability of residual rutile (with low $\delta^{98/95}Mo$) in the eclogite crust during subduction because of the strong partitioning of the lighter Mo isotopes in rutile (Chen et al., 2019; Freymuth et al., 2015). In this "reactive channelized flow" model, serpentinite-derived fluids ascend through the overlying mafic crustal section and react with residual rutile, leaving the fluids exiting the mafic crustal section isotopically heavy (Chen et al., 2019; Freymuth et al., 2015; Villalobos-Orchard et al., 2020). The ascending fluids then carry the high $\delta^{98/95}Mo$ signature into the hot mantle wedge and cause partial melting (Figure 6a). The combined Mo and Pb data in our samples support this notion and suggest that the reactive channelized flow model can explain the Mo isotope systematics in the EVF and CKD basalts. In this respect, it is worth emphasizing that the Pb isotope composition of the EVF and CKD basalts is determined by the source of the slab fluid (i.e., the dehydrating lithospheric mantle) and/or equilibration of the fluid with unaltered oceanic crust during its passage upwards, as both have the same Hawaii-type Pb isotopic composition (see above and Figure 5). At the same time, their Mo isotope composition is the result of an isotope fractionation process that operated during the reactive flow of the fluid released from the underlying serpentinized mantle. As such, a decoupling of both isotope systems would be expected and is, in fact, observed in our data set (Figure S3 in Supporting Information S1). In addition, the fractionation of Mo isotopes between the residual slab and the slab fluid is accompanied by an increase in the Pb and Mo concentrations in the passing fluid (i.e., decreasing its Ce/Mo and Ce/Pb) due to the fluid mobility of both elements (see above), leading to the observed trends between $\delta^{98/95}Mo$ and Ce/Mo, as well as Ce/Pb (Figure 4).

Previous workers have argued for models whereby slab fluids ultimately originate in the hydrated part of the subducted crust (Churikova, Wörner, Mironov, & Kronz, 2007; Churikova et al., 2001; Dorendorf, Wiechert, & Wörner, 2000; H. Liu et al., 2020; Shu et al., 2022). Yet, the two seemingly contrasting models of fluid sources may not be mutually exclusive. In fact, it is more than likely that there is more than one fluid source in such complex subduction zone systems like the Kamchatka arc (also see Rojas-Kolomiets et al., 2023). Churikova, Wörner, Mironov, and Kronz (2007) identified multiple fluid compositions involved in the petrogenesis of Kamchatka arc basalts. This is in line with our view that chalcophile element concentrations as well as the Li and Tl isotope and LILE systematics (Churikova, Wörner, Mironov, & Kronz, 2007; H. Liu et al., 2020; Shu et al., 2022) are most likely controlled by different fluid sources within the Kamchatka system compared to that controlling the Mo and Pb isotope systems (see above and Figure 4c). On the other side of the spectrum, Ahmad et al. (2021) and Rojas-Kolomiets et al. (2023) have recently suggested a model whereby slab fluids with a high

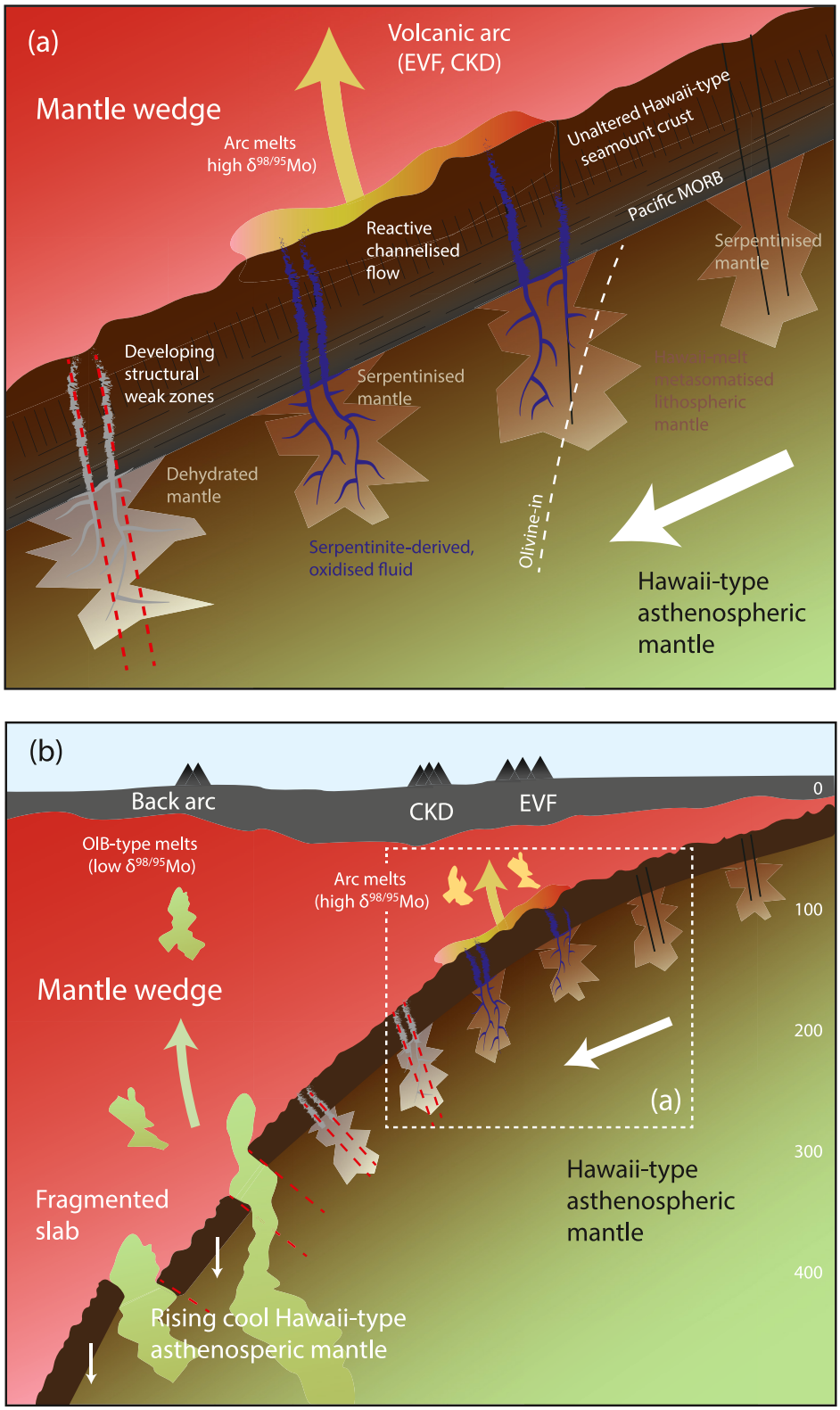
(a)
Volcanic arc
(EVF, CKD)
Mantle wedge
Arc melts
high δ98/95Mo)
Unaltered Hawaii-type
seamount crust
Pacific MORB
Reactive
channelised
flow
Serpentinised
mantle
Developing
structural
weak zones
Serpentinised
mantle
Hawaii-melt
metasomatised
lithospheric
mantle
Dehydrated
mantle
Olivine-in
Serpentinite-derived,
oxidised fluid
Hawaii-type
asthenospheric
mantle
(b)
Back arc
CKD
EVF
0
OIB-type melts
(low δ98/95Mo)
Arc melts
(high δ98/95Mo)
100
Mantle wedge
200
(a)
300
Hawaii-type
asthenospheric
mantle
Fragmented
slab
400
Rising cool Hawaii-type
asthenosperic mantle

Figure 6.

$\delta^{98/95}$Mo signature directly emanate from a serpentinized arc mantle. Questioning the reactive channelized flow model, they argue that the rutile formation in the subducting crust may occur early during the dehydration phase of the subducting serpentine mantle. This would prematurely lock up Mo into rutile thus rendering the reactive channelized flow model unlikely. Yet, such notion would necessitate quantitative redistribution of Mo into rutile to occur well before flushing of the subducting oceanic crust with serpentine-derived fluids as well as an inert behavior of rutile to mineral-fluid isotopic exchange during the succedent fluid flushing. In addition, it would also require the serpentinite-derived fluid to be void of any Mo. While this view may have some merit, it nevertheless relies on a series of assumptions that need to be verified. Based on our observations and interpretations presented above, we find the reactive channelized flow model to be the most likely explanation for the observed Mo isotope systematic in the Kamchatka arc basalts.

4.3. A Common Mo Isotope Slab Fluid Composition in the Izu and Kamchatka Arcs

The trend between $\delta^{98/95}$Mo and Ce/Pb defined by samples from the Izu arc and the EVF and CKD from the Kamchatka arc (Figure 4) approaches a maximum value of $\delta^{98/95}$Mo = 0.1–0.25‰ at a hypothetical, near-zero Ce/Pb value; that is, representing the "pure" Mo endmember fluid composition (see Villalobos-Orchard et al., 2020). This suggests that the Mo isotope fluid composition emerging from the subducted mafic oceanic crust in the two arc systems along the Western Pacific margin and ca. 3,700 km apart is surprisingly uniform. The Mo isotopic composition and concentration in the fluid passing through the subducted mafic oceanic crust are dominated primarily by interaction with rutile-bearing, subducted basaltic crust at eclogite facies (Chen et al., 2019; Freymuth et al., 2015; Villalobos-Orchard et al., 2020). The latter is likely to have a uniform petrological composition (in particular the presence of metamorphic rutile) and can explain, why the Mo isotope composition of slab fluids from sediment-poor subduction zone systems appears to be rather constant. If confirmed, a uniform fluid Mo composition emerging from the mafic portions of the subducted crust may ultimately be assumed for Mo mass balance calculations in other subduction zones that may also involve additional Mo sources, that is, subducted clastic and chemical sediments and crustal melts (e.g., Fang et al., 2022; Freymuth et al., 2016; Gaschnig et al., 2017; H. Q. Liu et al., 2022; Yu et al., 2022; Zhang et al., 2020).

4.4. An Enriched Mantle Source for the Back Arc Basalts

In contrast to the EVF and CKD lavas, the Ce/Pb and Ce/Mo values in back arc samples approach typical mantle values that are ca. 25 and 32, respectively (Gale et al., 2013; Hofmann et al., 1986; Newsom et al., 1986; Salters & Stracke, 2004). This suggests a waning influence of Mo and Pb from slab-derived fluid on the back arc mantle source composition. Back arc samples also display a considerable range in $(Nb/Zr)_{PUM}$ at rather constant $\delta^{98/95}$Mo (Figure 4d) and have lower $(Rb/La)_{PUM}$ and higher $(Nb/La)_{PUM}$ than EVF and CKD basalts (Figure 2; Figure S4 in Supporting Information S1). In addition, $^{143}Nd/^{144}Nd$ ratios are considerably lower in back arc samples compared to EVF and CKD lavas and MORB (Figure 3), pointing towards a long-term enrichment of incompatible elements in the back arc mantle source. These observations indicate an increasing dominance of an enriched mantle component on the composition of the back arc basalts (cf. Churikova et al., 2001; H. Liu et al., 2020; Münker et al., 2004), although slab fluid-impregnated mantle is still present in the back arc as evidenced by some back arc samples having $\delta^{98/95}$Mo, $(Rb/La)_{PUM}$, Ba/Th, $^{143}Nd/^{144}Nd$ and $(Nb/La)_{PUM}$ comparable to samples from the EVF and CKD (Figures 3 and 4; Figure S4 in Supporting Information S1). However, back arc samples with the most pronounced enriched mantle signature ($^{143}Nd/^{144}Nd < 0.513000$) also have high $(Nb/Zr)_{PUM}$ (i.e., >1.4) and average $\delta^{98/95}$Mo values (−0.31 to −0.18‰) that are slightly lower than the depleted mantle value and the majority of the arc basalts.

Such an enriched mantle component could be of "enigmatic origin," that is, represent ambient enriched mantle components within the upper mantle (Churikova et al., 2001). Recent studies revealed that MORB samples

Figure 6. A conceptual model illustrating the magmatic and structural processes that can reconcile the isotopic and geochemical composition of basaltic lavas in the Kamchatka subduction zone. Not to scale. (a) Reactive channelized flow model modified after Chen et al. (2019) and Spandler and Pirard (2013). Dehydration of subducted serpentinite lithospheric, followed by the interaction of fluids with rutile-bearing subducted oceanic crust can explain the combined Mo and Pb isotope and fluid-mobile element composition of Eastern Volcanic Front (EVF) and Central Kamchatka Depression (CKD) lavas. Prograde decomposition of serpentine in lithospheric mantle causes the formation of structural weak zones in the subducted slab (Craiu et al., 2022). (b) At high mantle depths (>300 km), structural failure of the slab due to the change from horizontal compression to vertical extension in the slab (Craiu et al., 2022), and possibly aided by progressive heating and additional loading from the heavy Hawaii-Emperor Seamount Chain eclogite crust, causes fragmentation of the slab. This allows the Hawaii-type asthenospheric mantle to leak into the Kamchatka arc mantle wedge, forming a source component of the back arc basalts. However, this asthenosphere may be too cool to initiate partial melting of eclogite crust (i.e., adakite formation) during passage. See text for further discussion.

comprising an enriched component have high $\delta^{98/95}$Mo values (Bezard et al., 2016; Chen et al., 2022), whereas ocean island basalts appear to have $\delta^{98/95}$Mo values lower than the average MORB value (Gaschnig et al., 2021b) that is similar to the values that we observe for the back arc basalts. For the remainder of this discussion, we will therefore focus on exploring more detailed models of the nature and origin of the enriched mantle component.

4.5. Origin of the Enriched Back Arc Mantle Component

4.5.1. Incorporation of a Hawaii Plume Component

There is considerable overlap between data for the back arc samples and data for modern ocean island basalts from Hawaii in terms of several key trace element ratios as well as $^{206}Pb/^{204}Pb$-$^{208}Pb/^{204}Pb$ isotope ratios (Figures 4 and 5; Figures S1 and S2 in Supporting Information S1). The match extends to Mo isotopes with the average and range of data for Hawaiian samples overlapping with that of the back arc samples at $^{143}Nd/^{144}Nd < 0.513030$ (Figure 3). This suggests that the back arc mantle source would be compositionally consistent with a Hawaii-type enriched mantle component. The Hawaii-Emperor Seamount Chain, currently being subducted below Kamchatka (Figure 1), is the surface expression of a long-lived mantle plume currently residing underneath the Hawaii archipelago (Clague & Brent Dalrymple, 1994; Regelous et al., 2003; Tatsumoto, 1978). Thus, the presence of an Hawaii-type enriched component in the back arc region of the Kamchatka arc is more than likely. Notably, all three units (EVF, CKD, back arc) have near-identical $^{206,208}Pb/^{204}Pb$ compositions of Hawaii-type heritage (Figure 5). The most straight-forward explanation for this is that the original Pb isotope composition of the Kamchatka arc mantle is quantitatively overprinted by a Hawaii-type slab fluid component (see above). The latter seems feasible given that slab-controlled Pb isotope budgets in subduction zones have been reported before (e.g., Straub et al., 2010). Adding a Hawaii-type enriched mantle as an additional component to the mantle source of the back arc lavas would, therefore, not result in a change of the Pb isotope composition of this mixture. At the same time, the $^{143}Nd/^{144}Nd$ isotope composition of the Kamchatka arc mantle (as gauged by data from the EVF and CKD) and the Hawaii mantle are different (Figure 3) because Nd is not transported in a slab fluid. As such, mixing between a Kamchatka arc mantle and an Hawaii-type enriched mantle to produce the back arc lavas does result in the observed variation of $^{143}Nd/^{144}Nd$ in the back arc basalts. Yet, all of this raises the question of how an Hawaii-type mantle component could contribute to the source of the back arc basalts that originated in the mantle wedge above the subducted plate.

4.5.2. Slab Window Formation and Associated Asthenosphere Mantle Corner Flow

To the East of Kamchatka, the Northwest-ward subducting Pacific plate is separated from the North American plate by a Northwest trending transform fault that continues into the trench of the subduction zone underneath Kamchatka (Figure 1). Here, the Eurasian, North American and Pacific plates form a triple junction at an angle of almost 90°. At this point, seismic data indicate that North of the triple point no subduction occurs (Davaille & Lees, 2004; Yogodzinski et al., 2001). Based on geophysical, geochemical and thermal models, it has been proposed that a slab window has opened within the subducting Pacific plate along the subducted transform fault at the Kamchatka-Aleutian junction (Yogodzinski et al., 2001). This slab window could allow the subducted Pacific mantle—and with it an enriched Hawaii-type mantle component—to enter the Kamchatka arc mantle wedge. Low-degree melting of the enriched Hawaii-type components contained in this mantle could then explain the observed enriched isotope and trace element signatures of the back arc basalts (see above). However, this would require the flow of Hawaii-type asthenospheric mantle to remain focused toward the back arc region of the Kamchatka system over a distance of >200 km away from the slab window to reconcile the observed Mo, Pb, and Nd isotopes as well as trace element composition of the back arc basalts.

4.5.3. Slab Melts From Subducted Crust in the Back Arc Mantle Source

Partial melts of subduction-modified crust have been hypothesized to explain the Mo isotope composition in arc lavas from the Mariana arc (cf. H. Y. Li et al., 2021b). Given its high age, the Hawaii-Emperor Seamount Chain crust, currently being subducted in the Kamchatka arc, is too cold to partially melt at a distance of >200 km away from the slab window (see above) (Figure 1). On the other hand, any partial melts generated directly along the edges of the subducted Pacific plate close to this presumed slab window would have a Pacific-type Pb isotope composition, unlike the Hawaii-like Pb isotope composition observed for the back arc basalts (Figure 5). Such slab melts would also have an adakitic trace element signature (high Sr/Y, LREE/HREE and Dy/Yb values), which is not observed in the back arc basalts (see above and Churikova et al., 2001). We also observe elevated

$\delta^{98/95}$Mo in purported partial melts of the residual subducting slab, that is, the three adakitic andesite samples from the NCKD (Table S1), where slab edge melting has previously been proposed (Yogodzinski et al., 2001). This contrasts the low $\delta^{98/95}$Mo values in the back arc basalts. It thus seems unlikely that the addition of partial melts from the subducted oceanic crust contributed to the trace element, radiogenic isotope and Mo isotope budget of the back arc mantle source.

4.5.4. Deep-Mantle Slab Fragmentation

Because serpentine has a lower density than olivine, serpentinization of mantle peridotite causes a ca. 50% volume increase that can lead to stress build-up and cracking (Evans, 2010; Jamtveit et al., 2008; Macdonald & Fyfe, 1995; O'Hanley, 1992). The serpentinization of the lithospheric oceanic mantle during incipient subduction is most likely confined to areas below deep-running fault zones within the oceanic crust (e.g., Spandler & Pirard, 2013). As such, the serpentinized lithospheric mantle volumes (Figure 6) must represent localized structural weak points within the subducted lithosphere, even before entering the subduction zone. In turn, consecutive volume decrease accompanying prograde dehydration at high mantle depths must aggravate the structural weakness of the subducted lithosphere. In fact, Craiu et al. (2022) recently found that dehydration of serpentinite in the subducted slab can cause an anisotropic volume change within the serpentinite mantle domains. Together with the rotation of the stress field from horizontal compression at shallow levels to vertical extension in the deep mantle during subduction (Figure 6b), the dehydration of the lithospheric mantle can result in fault reactivation, strain localization, structural weakening of the slab, and eventually vertical slab detachment (Craiu et al., 2022). In addition, model results suggest that the lithospheric mantle section of a ca. 90 Ma old subducted slab at >200 km mantle depths reaches temperatures of >700°C (Rupke, 2004) further weakening the structural cohesion of the subducted lithosphere. In the case of the subduction of the Hawaii-Emperor Seamount Chain in the Kamchatka arc, loading of the subducted lithospheric mantle by the overlying, high-density eclogite crust—much thicker than the normal oceanic crust—may add more localized and vertical structural stress to initiate structural failure and fragmentation of the subducted slab. We therefore hypothesize that a loss of structural integrity of the subducted Hawaii-Emperor Seamount Chain lithosphere at >300–400 km mantle depth (i.e., the depth of the slab surface under the back arc) may cause localized slab tearing, allowing asthenospheric Hawaii plume mantle to leak into the overlying subduction-modified Kamchatka arc wedge (Figure 6b). A contribution from leaked Hawaii-type mantel material underneath the back arc area to the back arc mantle source would be consistent with the isotopic and geochemical observations for the back arc basalts described above. This would also explain the unusual presence of increased volcanic activity so far behind the active volcanic front in absence of any major structural extension (the latter being concentrated in the CKD further toward the trench, Figure 1). At a depth of >300–400 km underneath the back arc area, the subducted slab is most likely completely dehydrated and mineralogically and geochemically too "inert" to further contribute any fusible components to the arc mantle. This is because under these high-pressure conditions (i.e., at 400 km mantle depth), the dry solidus of the vapor-free eclogite system lies at temperatures well above 1,300°C (Petermann & Hirschmann, 2003). Given that the subducted Hawaii-type asthenosphere mantle is likely to be comparatively cool, with temperatures close to the normal oceanic geotherm (i.e., <1,300°C, representing mantle material residing at shallow mantle levels for >90 million years), it may not be possible to produce partial melts from the overlying subducted fluid-depleted crust, even when the Hawaii-type asthenospheric mantle passes through the fragmented lithosphere (Figure 6b). The latter may also explain why distinct "adakite-like" signatures are missing in the Kamchatka back arc basalts.

We acknowledge that, so far, independent geophysical evidence to verify this notion for the Kamchatka arc system is missing; yet would like to point out that the localized fragmentation of the subducted slab along the subducted Hawaii-Emperor Seamount Chain may not be resolvable by seismic data (Figure 6). Also, such a process may or may not be distinctly unique to the Kamchatka arc owing to the generally high age and structural rigidness of the subducted lithosphere (i.e., >90 Ma) combined with the presence of a thick and heavy subducted seamount chain crust (i.e., the Hawaii-Emperor Seamount Chain), as well as the large isotopic and geochemical contrast between an in-leaking mantle (i.e., Hawaii asthenosphere) and the arc mantle.

5. Conclusions

In basalts from EVF and CKD, typical indicators of slab fluids, that is, Ce/Pb, Ce/Mo, and Ba/Th, co-vary with $\delta^{98/95}$Mo indicating that the Mo isotope composition in these rocks is dominated by a Mo-rich fluid component. In these plots, data for arc basalts from Izu and Kamchatka fall on the same trends suggesting that the subduction zone fluids in these two sediment-depleted arc systems have a rather uniform $\delta^{98/95}$Mo composition.

Back arc basalts show a waning influence of the slab fluid component and an increasing dominance of an enriched mantle component as inferred from systematic variations in $^{143}Nd/^{144}Nd$, $(Nb/Zr)_{PUM}$, along with other tracers of mantle enrichment, such as $(La/Sm)_{CI}$ and $(Nb/La)_{PUM}$. Notably, trends of these tracers with $\delta^{98/95}Mo$ point toward a Hawaii-type composition of such an enriched mantle component.

The mechanism for transferring an Hawaii-type signature into the Kamchatka back arc region remains open but can be explained by projected influx of Hawaii-type asthenospheric mantle through a slab window North of the path of the subducted Hawaii-Emperor Seamount Chain. Alternatively, the fragmentation of the subducted slab following structural failure at high mantle depths may allow cool Hawaii-type asthenospheric mantle to enter the mantle wedge directly below the back arc region. Independent verification of the latter model strongly depends on a better understanding of the physical properties of subducted oceanic lithosphere into the deeper mantle (i.e., beyond 300 km depth). However, in lieu of a better explanation for the involvement of a Hawaii-type mantle component in the Kamchatka back arc basalts, the slab fragmentation model remains our preferred option.

Data Availability Statement

Molybdenum isotope data for basalts from the Kamchatka subduction zone system as well as complementary Nd isotope and trace element data acquired in this study are provided in Table S1 and are archived at the Göttingen Research Online (GRO) data repository at Willbold (2023).

Acknowledgments
The authors would like to thank S. Metje for help in the clean room. G. Wörner and R. Bezard are thanked for fruitful discussions and comments on the manuscript as well as Q. Ahmad and an anonymous reviewer for detailed and constructive reviews. G. Wörner kindly made available the samples of this study. D. Hoffmann is thanked for support with mass spectrometry and clean lab maintenance. MW acknowledges support from DFG Grant WI 3579/5-1. Open Access funding enabled and organized by Projekt DEAL. We acknowledge support by the Open Access Publication Funds of the University of Göttingen.

References

Ahmad, Q., Wille, M., König, S., Rosca, C., Hensel, A., Pettke, T., & Hermann, J. (2021). The Molybdenum isotope subduction recycling conundrum: A case study from the Tongan subduction zone, Western Alps and Alpine Corsica. *Chemical Geology*, *576*, 120231. https://doi.org/10.1016/j.chemgeo.2021.120231

Ahmad, Q., Wille, M., Rosca, C., Labidi, J., Schmid, T., Mezger, K., & König, S. (2022). Molybdenum isotopes in plume-influenced MORBs reveal recycling of ancient anoxic sediments. *Geochemical Perspectives Letters*, *23*, 43–48. https://doi.org/10.7185/geochemlet.2236

Avanzinelli, R., Prytulak, J., Skora, S., Heumann, A., Koetsier, G., & Elliott, T. (2012). Combined ^{238}U–^{230}Th and ^{235}U–^{231}Pa constraints on the transport of slab-derived material beneath the Mariana Islands. *Geochimica et Cosmochimica Acta*, *92*, 308–328. https://doi.org/10.1016/j.gca.2012.06.020

Balesta, S. T. (1991). Earth crust structure and magma chambers of the areas of present Kamchatka volcanism. In S. A. Fedotov, & Y. P. Masurenkov (Eds.), *Active volcanoes of Kamchatka* (pp. 36–45).

Bali, E., Keppler, H., & Audetat, A. (2012). The mobility of W and Mo in subduction zone fluids and the Mo–W–Th–U systematics of island arc magmas. *Earth and Planetary Science Letters*, *351–352*, 195–207. https://doi.org/10.1016/j.epsl.2012.07.032

Bezard, R., Fischer-Gödde, M., Hamelin, C., Brennecka, G. A., & Kleine, T. (2016). The effects of magmatic processes and crustal recycling on the molybdenum stable isotopic composition of Mid-Ocean Ridge Basalts. *Earth and Planetary Science Letters*, *453*, 171–181. https://doi.org/10.1016/j.epsl.2016.07.056

Bigeleisen, J., & Mayer, M. G. (1947). Calculation of equilibrium constants for isotopic exchange reactions. *The Journal of Chemical Physics*, *15*(5), 261–267. https://doi.org/10.1063/1.1746492

Burkhardt, C., Hin, R. C., Kleine, T., & Bourdon, B. (2014). Evidence for Mo isotope fractionation in the solar nebula and during planetary differentiation. *Earth and Planetary Science Letters*, *391*, 201–211. https://doi.org/10.1016/j.epsl.2014.01.037

Casalini, M., Avanzinelli, R., Tommasini, S., Elliott, T., & Conticelli, S. (2019). Ce/Mo and molybdenum isotope systematics in subduction-related orogenic potassic magmas of Central-Southern Italy. *Geochemistry, Geophysics, Geosystems*, *20*(6), 2753–2768. https://doi.org/10.1029/2019gc008193

Chen, S., Hin, R. C., John, T., Brooker, R., Bryan, B., Niu, Y., & Elliott, T. (2019). Molybdenum systematics of subducted crust record reactive fluid flow from underlying slab serpentine dehydration. *Nature Communications*, *10*(1), 4773. https://doi.org/10.1038/s41467-019-12696-3

Chen, S., Sun, P., Niu, Y., Guo, P., Elliott, T., & Hin, R. C. (2022). Molybdenum isotope systematics of lavas from the East Pacific Rise: Constraints on the source of enriched mid-ocean ridge basalt. *Earth and Planetary Science Letters*, *578*, 117283. https://doi.org/10.1016/j.epsl.2021.117283

Churikova, T., Dorendorf, F., & Wörner, G. (2001). Sources and fluids in the mantle wedge below Kamchatka, evidence from across-arc geochemical variation. *Journal of Petrology*, *42*(8), 1567–1593. https://doi.org/10.1093/petrology/42.8.1567

Churikova, T., Wörner, G., Eichelberger, J., & Ivanov, B. (2007). Minor- and trace element zoning in plagioclase from Kizimen Volcano, Kamchatka: Insights on the magma chamber processe. In J. Eichelberger, E. Gordeev, P. Izbekov, M. Kasahara, & J. Lees (Eds.), *Volcanism and subduction: The Kamchatka region*. American Geophysical Union.

Churikova, T., Wörner, G., Mironov, N., & Kronz, A. (2007). Volatile (S, Cl and F) and fluid mobile trace element compositions in melt inclusions: Implications for variable fluid sources across the Kamchatka arc. *Contributions to Mineralogy and Petrology*, *154*(2), 217–239. https://doi.org/10.1007/s00410-007-0190-z

Clague, D. A., & Brent Dalrymple, G. (1994). Tectonics, geochronology, and origin of the Hawaiian-emperor volcanic chain. In *A natural history of the Hawaiian Islands* (pp. 5–40). https://doi.org/10.1515/9780824844264-003

Craiu, A., Ferrand, T. P., Manea, E. F., Vrijmoed, J. C., & Marmureanu, A. (2022). A switch from horizontal compression to vertical extension in the Vrancea slab explained by the volume reduction of serpentine dehydration. *Scientific Reports*, *12*(1), 22320. https://doi.org/10.1038/s41598-022-26260-5

Davaille, A., & Lees, J. M. (2004). Thermal modeling of subducted plates: Tear and hotspot at the Kamchatka corner. *Earth and Planetary Science Letters*, *226*(3–4), 293–304. https://doi.org/10.1016/j.epsl.2004.07.024

Davidson, J., Turner, S., & Plank, T. (2013). Dy/Dy*: Variations arising from mantle sources and petrogenetic processes. *Journal of Petrology*, *54*(3), 525–537. https://doi.org/10.1093/petrology/egs076

Dorendorf, F., Churikova, T., Koloskov, K., & Wörner, G. (2000). Late Pleistocene to Holocene activity at Bakening volcano and surrounding monogenetic centers (Kamchatka): Volcanic geology and geochemical evolution. *Journal of Volcanology and Geothermal Research*, *104*(1–4), 131–151. https://doi.org/10.1016/s0377-0273(00)00203-1

Dorendorf, F., Wiechert, U., & Wörner, G. (2000). Hydrated sub-arc mantle: A source for the Kluchevskoy volcano, Kamchatka/Russia. *Earth and Planetary Science Letters*, *175*(1–2), 69–86. https://doi.org/10.1016/s0012-821x(99)00288-5

Elliott, T., Blichert-Toft, J., Heumann, A., Koetsier, G., & Forjaz, V. (2007). The origin of enriched mantle beneath Sao Miguel, Azores. *Geochimica et Cosmochimica Acta*, *71*(1), 219–240. https://doi.org/10.1016/j.gca.2006.07.043

Elliott, T., Plank, T., Zindler, A., White, W., & Bourdon, B. (1997). Element transport from slab to volcanic front at the Mariana arc. *Journal of Geophysical Research*, *102*(B7), 14991–15019. https://doi.org/10.1029/97jb00788

Evans, B. W. (2010). The serpentinite multisystem revisited: Chrysotile is metastable. *International Geology Review*, *46*(6), 479–506. https://doi.org/10.2747/0020-6814.46.6.479

Fang, W., Dai, L.-Q., Zheng, Y.-F., & Zhao, Z.-F. (2022). Basalt Mo isotope evidence for crustal recycling in continental subduction zone. *Geochimica et Cosmochimica Acta*, *334*, 273–292. https://doi.org/10.1016/j.gca.2022.08.008

Freymuth, H., Elliott, T., van Soest, M., & Skora, S. (2016). Tracing subducted black shales in the Lesser Antilles arc using molybdenum isotope ratios. *Geology*, *44*(12), 987–990. https://doi.org/10.1130/g38344.1

Freymuth, H., Vils, F., Willbold, M., Taylor, R. N., & Elliot, T. (2015). Molybdenum mobility and isotopic fractionation during subduction at the Mariana arc. *Earth and Planetary Science Letters*, *432*, 176–186. https://doi.org/10.1016/j.epsl.2015.10.006

Gale, A., Dalton, C. A., Langmuir, C. H., Su, Y., & Schilling, J.-G. (2013). The mean composition of ocean ridge basalts. *Geochemistry, Geophysics, Geosystems*, *14*(3), 489–518. https://doi.org/10.1029/2012gc004334

Gaschnig, R. M., Rader, S. T., Reinhard, C. T., Owens, J. D., Planavsky, N., Wang, X., et al. (2021a). Behavior of the Mo, Tl, and U isotope systems during differentiation in the Kilauea Iki lava lake. *Chemical Geology*, *574*, 120239. https://doi.org/10.1016/j.chemgeo.2021.120239

Gaschnig, R. M., Reinhard, C. T., Planavsky, N. J., Wang, X., Asael, D., & Chauvel, C. (2017). The molybdenum isotope system as a tracer of slab input in subduction zones: An example from Martinique, Lesser Antilles arc. *Geochemistry, Geophysics, Geosystems*, *18*(12), 4674–4689. https://doi.org/10.1002/2017gc007085

Gaschnig, R. M., Reinhard, C. T., Planavsky, N. J., Wang, X., Asael, D., & Jackson, M. G. (2021b). The impact of primary processes and secondary alteration on the stable isotope composition of ocean island basalts. *Chemical Geology*, *581*, 581. https://doi.org/10.1016/j.chemgeo.2021.120416

Geist, E. L., & Scholl, D. W. (1994). Large-scale deformation related to the collision of the Aleutian Arc with Kamchatka. *Tectonics*, *13*(3), 538–560. https://doi.org/10.1029/94tc00428

Gill, J. B. (1981). Bulk chemical composition of orogenic andesites. In *Orogenic andesites and plate tectonics* (pp. 97–167). Springer.

Gorbatov, A. V. (1997). *Sismicidad y estructura de la zona de subduction de Kamchatka* (p. 144). UNAM.

Gorelchik, V. I., Shirokov, V. A., Firstov, P. P., & Chubarova, O. S. (1997). Shiveluch volcano: Seismicity, deep structure and forecasting eruptions (Kamchatka). *Journal of Volcanology and Geothermal Research*, *78*(1–2), 121–132. https://doi.org/10.1016/s0377-0273(96)00108-4

Greaney, A. T., Rudnick, R. L., Gaschnig, R. M., Whalen, J. B., Luais, B., & Clemens, J. D. (2018). Geochemistry of molybdenum in the continental crust. *Geochimica et Cosmochimica Acta*, *238*, 36–54. https://doi.org/10.1016/j.gca.2018.06.039

Greber, N. D., Puchtel, I. S., Nägler, T. F., & Mezger, K. (2015). Komatiites constrain molybdenum isotope composition of the Earth's mantle. *Earth and Planetary Science Letters*, *421*, 129–138. https://doi.org/10.1016/j.epsl.2015.03.051

Green, T. H., & Adam, J. (2003). Experimentally-determined trace element characteristics of aqueous fluid from partially dehydrated mafic oceanic crust at 3.0 GPa, 650–700°C. *European Journal of Mineralogy*, *15*(5), 815–830. https://doi.org/10.1127/0935-1221/2003/0015-0815

Hawkesworth, C. J., Hergt, J. M., Ellam, R. M., & McDermott, F. (1991). Element fluxes associated with subduction related magmatism. *Philosophical Transactions of the Royal Society*, *335*, 393–405.

Hin, R. C., Hibbert, K. E. J., Chen, S., Willbold, M., Andersen, M. B., Kiseeva, E. S., et al. (2022). The influence of crustal recycling on the molybdenum isotope composition of the Earth's mantle. *Earth and Planetary Science Letters*, *595*, 117760. https://doi.org/10.1016/j.epsl.2022.117760

Hofmann, A. W., Jochum, K. P., Seufert, H. M., & White, W. M. (1986). Nb and Pb in oceanic basalts: New constraints on mantle evolution. *Earth and Planetary Science Letters*, *79*(1–2), 33–45. https://doi.org/10.1016/0012-821x(86)90038-5

Ishikawa, T., Tera, F., & Nakazawa, T. (2001). Boron isotope and trace element systematics of the three volcanic zones in the Kamchatka arc. *Geochimica et Cosmochimica Acta*, *65*(24), 4523–4537. https://doi.org/10.1016/s0016-7037(01)00765-7

Jamtveit, B., Putnis, C. V., & Malthe-Sørenssen, A. (2008). Reaction induced fracturing during replacement processes. *Contributions to Mineralogy and Petrology*, *157*(1), 127–133. https://doi.org/10.1007/s00410-008-0324-y

Kepezhinkas, P., McDermott, F., Defant, M. J., Hochstaedter, A., Drummond, M. S., Hawkesworth, C., et al. (1997). Trace element and Sr-Nd-Pb isotopic constraints on a three-component model of Kamchatka arc petrogenesis. *Geochimica et Cosmochimica Acta*, *61*(3), 577–600. https://doi.org/10.1016/s0016-7037(96)00349-3

Keppler, H. (1996). Constraints from the partitioning experiments on the composition of subduction-zone fluids. *Nature*, *380*(6571), 237–240. https://doi.org/10.1038/380237a0

Kersting, A. B., & Arculus, R. J. (1995). Pb isotope composition of Klyuchevskoy volcano, Kamchatka and North Pacific sediments: Implications for magma genesis and crustal recycling in the Kamchatkan arc. *Earth and Planetary Science Letters*, *136*(3–4), 133–148. https://doi.org/10.1016/0012-821x(95)00196-j

König, S., Wille, M., Voegelin, A., & Schoenberg, R. (2016). Molybdenum isotope systematics in subduction zones. *Earth and Planetary Science Letters*, *447*, 95–102. https://doi.org/10.1016/j.epsl.2016.04.033

Le Maitre, R. W., Bateman, P., Dudek, A. J., & Keller, M. J. (1989). A classification of igneous rocks and glossary of terms.

Li, H.-Y., Li, J., Ryan, J. G., Li, X., Zhao, R.-P., Ma, L., & Xu, Y.-G. (2019). Molybdenum and boron isotope evidence for fluid-fluxed melting of intraplate upper mantle beneath the eastern North China Craton. *Earth and Planetary Science Letters*, *520*, 105–114. https://doi.org/10.1016/j.epsl.2019.05.038

Li, H. Y., Zhao, R. P., Li, J., Tamura, Y., Spencer, C., Stern, R. J., et al. (2021b). Molybdenum isotopes unmask slab dehydration and melting beneath the Mariana arc. *Nature Communications*, *12*(1), 6015. https://doi.org/10.1038/s41467-021-26322-8

Li, X., Yan, Q., Zeng, Z., Fan, J., Li, S., Li, J., et al. (2021a). Across-arc variations in Mo isotopes and implications for subducted oceanic crust in the source of back-arc basin volcanic rocks. *Geology*, *49*(10), 1165–1170. https://doi.org/10.1130/g48754.1

Liang, Y.-H., Halliday, A. N., Siebert, C., Fitton, J. G., Burton, K. W., Wang, K.-L., & Harvey, J. (2017). Molybdenum isotope fractionation in the mantle. *Geochimica et Cosmochimica Acta*, *199*, 91–111. https://doi.org/10.1016/j.gca.2016.11.023

Liu, H., Xiao, Y., Sun, H., Tong, F., Heuser, A., Churikova, T., & Wörner, G. (2020). Trace elements and Li isotope compositions across the Kamchatka arc: Constraints on slab-derived fluid sources. *Journal of Geophysical Research: Solid Earth*, *125*(5), e2019JB019237. https://doi.org/10.1029/2019jb019237

Liu, H.-Q., Li, J., Xu, Y.-G., Yumul, G. P., Knittel, U., Dimalanta, C. B., et al. (2022). Heavy Mo isotope composition of northern Bataan adakites, Philippines: Evidence for fore-arc subduction erosion? *Geology*, *51*(1), 49–53. https://doi.org/10.1130/g50465.1

Ma, L., Xu, Y.-G., Li, J., Chen, L.-H., Liu, J.-Q., Huang, X.-L., et al. (2022). Molybdenum isotopic constraints on the origin of EM1-type continental intraplate basalts. *Earth and Planetary Science Letters*, *317*, 255–268. https://doi.org/10.1016/j.gca.2021.11.013

Macdonald, A. H., & Fyfe, W. S. (1995). Rate of serpentinisation in seafloor environments. *Tectonophysics*, *116*(1–2), 123–135. https://doi.org/10.1016/0040-1951(85)90225-2

McCoy-West, A. J., Chowdhury, P., Burton, K. W., Sossi, P., Nowell, G. M., Fitton, J. G., et al. (2019). Extensive crustal extraction in Earth's early history inferred from molybdenum isotopes. *Nature Geoscience*, *12*(11), 946–951. https://doi.org/10.1038/s41561-019-0451-2

McCulloch, M. T., & Gamble, J. A. (1991). Geochemical and geodynamical constraints on subduction zone magmatism. *Earth and Planetary Science Letters*, *102*(3–4), 358–374. https://doi.org/10.1016/0012-821x(91)90029-h

Miller, D. M., Goldstein, S. L., & Langmuir, C. H. (1994). Cerium/lead and lead isotope ratios in arc magmas and the enrichment of lead in the continents. *Nature*, *368*(6471), 514–520. https://doi.org/10.1038/368514a0

Münker, C., Wörner, G., Yogodzinski, G., & Churikova, T. (2004). Behavior of high field strength elements in subduction zones: Constraints from Kamchatka-Aleutian arc lavas. *Earth and Planetary Science Letters*, *224*(3–4), 275–293. https://doi.org/10.1016/j.epsl.2004.05.030

Newsom, H. E., & Palme, H. (1984). The depletion of siderophile elements in the Earth's mantle: New evidence from molybdenum and tungsten. *Earth and Planetary Science Letters*, *69*(2), 354–364. https://doi.org/10.1016/0012-821x(84)90194-8

Newsom, H. E., White, W. M., Jochum, K. P., & Hofmann, A. W. (1986). Siderophile and chalcophile element abundances in oceanic basalts, Pb isotopic evolution and growth of the Earth's core. *Earth and Planetary Science Letters*, *80*(3–4), 299–313. https://doi.org/10.1016/0012-821x(86)90112-3

Norman, M. D., & Garcia, M. O. (1999). Primitive magmas and source characteristics of the Hawaiian plume: Petrology and geochemistry of shield picrites. *Earth and Planetary Science Letters*, *168*(1–2), 27–44. https://doi.org/10.1016/s0012-821x(99)00043-6

O'Hanley, D. S. (1992). Solution to the volume problem in serpentinisation. *Geology*, *20*(8), 705–708. https://doi.org/10.1130/0091-7613(1992)020<0705:sttvpi>2.3.co;2

O'Neill, H. S. C., & Eggins, S. M. (2002). The effect of melt composition on trace element partitioning: An experimental investigation of the activity coefficients of FeO, NiO, CoO, MoO_2 and MoO_3 in silicate melts. *Chemical Geology*, *186*(1–2), 151–181. https://doi.org/10.1016/s0009-2541(01)00414-4

Palme, H., & O'Neill, H. S. C. (2014). Cosmochemical estimates of mantle composition. In R. W. Carlson (Ed.), *Treatise on geochemistry* (2nd ed., pp. 1–39). Elsevier. https://doi.org/10.1016/b978-0-08-095975-7.00201-1

Pearce, J. A., & Peate, D. W. (1995). Tectonic implications of the composition of volcanic arc magma. *Annual Review of Earth and Planetary Sciences*, *23*(1), 251–285. https://doi.org/10.1146/annurev.ea.23.050195.001343

Petermann, M., & Hirschmann, M. M. (2003). Anhydrous partial melting experiments on MORB-like eclogite: Phase relations, phase compositions and mineral-melt partitioning of major elements at 2-3 GPa. *Journal of Petrology*, *44*(12), 2173–2201. https://doi.org/10.1093/petrology/egg074

Ranero, C. R., Phipps Morgan, J., McIntosh, K., & Reichert, C. (2003). Bending-related faulting and mantle serpentinization at the Middle America trench. *Nature*, *425*(6956), 367–373. https://doi.org/10.1038/nature01961

Regelous, M., Hofmann, A., Abouchami, W., & Galer, S. J. G. (2003). Geochemistry of lavas from the Emperor Seamounts, and the geochemical evolution of Hawaiian magmatism from 85 to 42Ma. *Journal of Petrology*, *44*(1), 113–140. https://doi.org/10.1093/petrology/44.1.113

Rojas-Kolomiets, E., Jensen, O., Bizimis, M., Yogodzinski, G., & Ackerman, L. (2023). Serpentinite fluids and slab-melting in the Aleutian arc: Evidence from molybdenum isotopes and boron systematics. *Earth and Planetary Science Letters*, *603*, 117970. https://doi.org/10.1016/j.epsl.2022.117970

Rudnick, R. L., & Gao, S. (2014). Composition of the continental crust. In H. D. Holland, & K. K. Turekian (Eds.), *Treatise on geochemistry* (2nd ed., pp. 1–51). Elsevier. https://doi.org/10.1016/b978-0-08-095975-7.00301-6

Rupke, L. (2004). Serpentine and the subduction zone water cycle. *Earth and Planetary Science Letters*, *223*(1–2), 17–34. https://doi.org/10.1016/j.epsl.2004.04.018

Salters, V. J. M., & Stracke, A. (2004). Composition of the depleted mantle. *Geochemistry, Geophysics, Geosystems*, *5*, 2003GC000597. https://doi.org/10.1029/2003gc000597

Shu, Y., Nielsen, S. G., Le Roux, V., Worner, G., Blusztajn, J., & Auro, M. (2022). Sources of dehydration fluids underneath the Kamchatka arc. *Nature Communications*, *13*(1), 4467. https://doi.org/10.1038/s41467-022-32211-5

Skora, S., & Blundy, J. (2010). High-pressure hydrous phase relations of radiolarian clay and implications for the involvement of subducted sediment in arc magmatism. *Journal of Petrology*, *51*(11), 2211–2243. https://doi.org/10.1093/petrology/egq054

Spandler, C., & Pirard, C. (2013). Element recycling from subducting slabs to arc crust: A review. *Lithos*, *170–171*, 208–223. https://doi.org/10.1016/j.lithos.2013.02.016

Stracke, A., Hofmann, A. W., & Hart, S. R. (2005). FOZO, HIMU and the rest of the mantle zoo. *Geochemistry, Geophysics, Geosystems*, *6*(5), 2004GC00824. https://doi.org/10.1029/2004gc000824

Straub, S. M., Goldstein, S. L., Class, C., Schmidt, A., & Gomez-Tuena, A. (2010). Slab and mantle controls on the Sr–Nd–Pb–Hf isotope evolution of the post 42 Ma Izu–Bonin volcanic arc. *Journal of Petrology*, *51*(5), 993–1026. https://doi.org/10.1093/petrology/egq009

Tatsumoto, M. (1978). Isotopic composition of lead in oceanic basalts and its implication to mantle evolution. *Earth and Planetary Science Letters*, *38*(1), 63–87. https://doi.org/10.1016/0012-821x(78)90126-7

Till, C. B., Grove, T. L., & Withers, A. C. (2011). The beginnings of hydrous mantle wedge melting. *Contributions to Mineralogy and Petrology*, *163*(4), 669–688. https://doi.org/10.1007/s00410-011-0692-6

Urey, H. C. (1947). The thermodynamic properties of isotopic substances. *Journal of the Chemical Society*, 562–581. https://doi.org/10.1039/jr9470000562

van Keken, P. E., Hacker, B. R., Syracuse, E. M., & Abers, G. A. (2011). Subduction factory: 4. Depth-Dependent flux of H_2O from subducting slabs worldwide. *Journal of Geophysical Research*, *116*(B1), B01401. https://doi.org/10.1029/2010jb007922

Villalobos-Orchard, J., Freymuth, H., O'Driscoll, B., Elliott, T., Williams, H., Casalini, M., & Willbold, M. (2020). Molybdenum isotope ratios in Izu arc basalts: The control of subduction zone fluids on compositional variations in arc volcanic systems. *Geochimica et Cosmochimica Acta*, *288*, 68–82. https://doi.org/10.1016/j.gca.2020.07.043

Voegelin, A. R., Pettke, T., Greber, N. D., von Niederhäusern, B., & Nägler, T. F. (2014). Magma differentiation fractionates Mo isotope ratios: Evidence from the Kos Plateau Tuff (Aegean Arc). *Lithos*, *190–191*, 440–448. https://doi.org/10.1016/j.lithos.2013.12.016

Volynets, A. O., Churikova, T. G., Wörner, G., Gordeychik, B. N., & Layer, P. (2009). Mafic Late Miocene–Quaternary volcanic rocks in the Kamchatka back arc region: Implications for subduction geometry and slab history at the Pacific–Aleutian junction. *Contributions to Mineralogy and Petrology*, *159*(5), 659–687. https://doi.org/10.1007/s00410-009-0447-9

Walowski, K. J., Wallace, P. J., Hauri, E. H., Wada, I., & Clynne, M. A. (2015). Slab melting beneath the Cascade Arc driven by dehydration of altered oceanic peridotite. *Nature Geoscience*, *8*(5), 404–408. https://doi.org/10.1038/ngeo2417

Willbold, M. (2023). 160423_2mw [Dataset]. GRO.data. https://doi.org/10.25625/P5BBFL

Willbold, M., & Elliott, T. (2017). Molybdenum isotope variations in magmatic rocks. *Chemical Geology*, *449*, 253–268. https://doi.org/10.1016/j.chemgeo.2016.12.011

Wille, M., Nebel, O., Pettke, T., Vroon, P. Z., König, S., & Schoenberg, R. (2018). Molybdenum isotope variations in calc-alkaline lavas from the Banda arc, Indonesia: Assessing the effect of crystal fractionation in creating isotopically heavy continental crust. *Chemical Geology*, *485*, 1–13. https://doi.org/10.1016/j.chemgeo.2018.02.037

Workman, R. K., & Hart, S. R. (2005). Major and trace element composition of the depleted MORB mantle (DMM). *Earth and Planetary Science Letters*, *231*(1–2), 53–72. https://doi.org/10.1016/j.epsl.2004.12.005

Yang, J., Siebert, C., Barling, J., Savage, P., Liang, Y.-H., & Halliday, A. N. (2015). Absence of molybdenum isotope fractionation during magmatic differentiation at Hekla volcano, Iceland. *Geochimica et Cosmochimica Acta*, *162*, 126–136. https://doi.org/10.1016/j.gca.2015.04.011

Yogodzinski, G. M., Lees, J. M., Churikova, T. G., Dorendorf, F., Wörner, G., & Volynets, O. A. (2001). Geochemical evidence for the melting of subducting oceanic lithosphere at plate edges. *Nature*, *409*(6819), 500–504. https://doi.org/10.1038/35054039

Yogodzinski, G. M., Kay, R. W., Volynets, O. N., Koloskov, A. V., & Kay, S. M. (1995). Magnesian andesite in the western Aleutian Komandorsky region: Implications for slab melting and processes in the mantle wedge. *GSA Bulletin*, *107*(5), 505–519. https://doi.org/10.1130/0016-7606(1995)107<0505:maitwa>2.3.co;2

Yu, Y., Huang, X.-L., Chung, S.-L., Li, J., Lai, Y.-M., Setiawan, I., & Sun, M. (2022). Molybdenum isotopic constraint from Java on slab inputs to subduction zone magmatism. *Earth and Planetary Science Letters*, *332*, 1–18. https://doi.org/10.1016/j.gca.2022.06.009

Zhang, Y., Yuan, C., Sun, M., Chen, M., Hong, L., Li, J., et al. (2019). Recycled oceanic crust in the form of pyroxenite contributing to the Cenozoic continental basalts in central Asia: New perspectives from olivine chemistry and whole-rock B–Mo isotopes. *Contributions to Mineralogy and Petrology*, *174*(10), 83. https://doi.org/10.1007/s00410-019-1620-4

Zhang, Y., Yuan, C., Sun, M., Li, J., Long, X., Jiang, Y., & Huang, Z. (2020). Molybdenum and boron isotopic evidence for carbon-recycling via carbonate dissolution in subduction zones. *Geochimica et Cosmochimica Acta*, *278*, 340–352. https://doi.org/10.1016/j.gca.2019.12.013

References From the Supporting Information

Bezard, R., & Guo, H. (2023). Fluid-melt Mo isotope fractionation: Implications for the $\delta^{98/95}$Mo of the upper crust. *Geochemical Perspectives Letters*, *26*, 25–30. https://doi.org/10.7185/geochemlet.2320

Hegner, E., Alexeiev, D. V., Willbold, M., Kröner, A., Topuz, G., & Mikolaichuk, A. V. (2019). Early Silurian tholeiitic-boninitic Mailisu ophiolite, South Tianshan, Kyrgyzstan: A geochemical record of subduction initiation. *International Geology Review*, *62*(3), 1–18. https://doi.org/10.1080/00206814.2019.1610670

Hegner, E., Rajesh, S., Willbold, M., Mueller, D., Joachimski, M., Hofmann, M., et al. (2020). Sediment-derived origin of the putative Munnar carbonatite, South India. *Journal of Asian Earth Sciences*, *200*, 104432. https://doi.org/10.1016/j.jseaes.2020.104432

Palme, H., Lodders, K., & Jones, A. (2014). Solar system abundances of the elements. In H. D. Holland, & K. K. Turekian (Eds.), *Treatise on geochemistry* (2nd ed., pp. 15–36). Elsevier. https://doi.org/10.1016/b978-0-08-095975-7.00118-2

Willbold, M., Hibbert, K., Lai, Y.-J., Freymuth, H., Hin, R. C., Coath, C., et al. (2016). High-precision mass-dependent molybdenum isotope variations in magmatic rocks determined by double-spike MC-ICP-MS. *Geostandards and Geoanalytical Research*, *40*(3), 389–403. https://doi.org/10.1111/ggr.12109